Inorganica Chimica Acta 423 (2014) 477–488

Contents lists available at ScienceDirect

Inorganica Chimica Acta

journal homepage: www.elsevier.com/locate/ica

Aliphatic dicarboxylate copper coordination polymers with 3-pyridylmethylnicotinamide: Effect of chain length and steric bulk on dimensionality

Maria D. Torres Salgado, Robert L. LaDuca *

Lyman Briggs College and Department of Chemistry, Michigan State University, East Lansing, MI 48825, USA

ARTICLE INFO

Article history:
Received 15 July 2014
Received in revised form 17 August 2014
Accepted 18 August 2014
Available online 16 September 2014

Keywords:
Copper
Dicarboxylate
Crystal structure
Coordination polymer
Antiferromagnetism

ABSTRACT

Hydrothermal reaction of divalent copper salts, aliphatic dicarboxylic acids, and 3-pyridylmethylnicotinamide (3-pmna) has afforded a series of coordination polymer solids that were characterized via single-crystal X-ray crystallography. A significant dependence of the dimensionality and topology of these materials on the part of aliphatic chain length and substituent was revealed. Both $[Cu_2(suc)_2(3\text{-pmna})]_n$ (**1**, suc = succinate) and its substituted congener $\{[Cu_2(dms)_2(3\text{-pmna})]\cdot 4H_2O\}_n$ (**2**, dms = 2,2-dimethylsuccinate) manifest $\{Cu_2(OCO)_4\}$ paddlewheel dimers, connected into chain motifs that are further linked by 3-pmna ligands into 2-D (4,4) grid networks. The enhanced steric bulk of the dms ligands in **2** impart larger interlamellar regions occupied by disordered water molecules. $\{[Cu_2(glu)_2(3\text{-pmna})]\cdot H_2O\}_n$ (**3**, glu = glutarate) has similar dimer-containing $[Cu_2(glu)_2]_n$ chain motifs, but retains a 1-D dimensionality due to bridging by *syn*-conformation 3-pmna ligands. $[Cu(2\text{-mglu})(3\text{-pmna})]_n$ (**4**, 2-mglu = 2-methylglutarate) features *anti-syn* $\{CuOCO\}_n$ chain patterns and a 3,5-connected $(3.5^2)(3^2 5^3 6^4 7)$ 2-D topology. $\{[Cu_2(adp)_2(3\text{-pmna})_2]\cdot H_2O\}_n$ (**5**, adp = adipate) exhibits 2-D $[Cu_2(adp)_2]_n$ layers, linked by *anti*-conformation 3-pmna ligands into a very rare 3-D 3,5-connected **hms** net with $(6^3)(6^9 8)$ topology. A minor 1-D chain product $\{[Cu_2(adp)_2(3\text{-pmna})]\cdot 0.25H_2O\}_n$ (**6**) was also isolated at higher temperature. Variable temperature magnetic susceptibility data for **5** indicates the presence of very weak antiferromagnetic coupling along its *anti-syn* bridged $\{CuOCO\}_n$ chains. Thermal properties of these new materials are also investigated.

1. Introduction

Investigations into the preparation, structural characterization, and properties of divalent metal coordination polymers continue apace after approximately two decades of consistent basic research. Hydrogen storage [1], selective absorbance [2], ion exchange [3], catalysis [4], luminescent sensing [5], and single molecular magnetism [6] are all enticing properties that provide tangible impetus for continued research efforts. The large majority of divalent metal coordination polymer crystalline solids are built from organic dicarboxylate ligands, which impart both the necessary charge balance and critical structural framework stability. Divalent copper coordination polymers of this type manifest a plethora of coordination polymer structural topologies [7]. This ion's flexible coordination preference and tendency to form clusters, along with specific donor dispositions and binding modes of the dicarboxylate components largely prevents *a priori* structure prediction in these materials, especially if neutral dipyridyl-type ligands are employed [8]. An additional means to enhance the topological scope of this class of crystalline solids involves the adjustment of chain length and steric bulk of aliphatic dicarboxylate ligands [9–12]. The conformational flexibility of the polymethylene chains of these ligands permits active response to specific supramolecular environments, while the presence of bulky alkyl group substituents can potentially restrict access to other possible conformations or binding modes during coordination polymer self-assembly.

The straight chain aliphatic dicarboxylate ligands succinate (suc) [9], glutarate (glu) [10], or adipate (adp) [11], in tandem with dipyridyl-type ligands, have afforded diverse topologies and metal aggregation modes in divalent copper coordination polymers. $\{[Cu(suc)(bpy)(H_2O)_2]\cdot 2H_2O\}_n$ (bpy = 4,4′-bipyridine) shows a 3-D non-interpenetrated 4-connected $7^5 9$ **qzd** topology [9a], while $\{[Cu(suc)(dpa)]\cdot 0.5H_2O\}_n$ (dpa = 4,4′-dipyridylamine) displays a 2-fold interpenetrated $6^5 8$ **cds** topology [9b]. Use of the sterically bulkier 2,2-dimethylsuccinate (dms) ligand in tandem with dpa

* Corresponding author at: Lyman Briggs College, E-30 Holmes Hall, Michigan State University, East Lansing, MI 48825, USA.
E-mail address: laduca@msu.edu (R.L. LaDuca).

http://dx.doi.org/10.1016/j.ica.2014.08.059
0020-1693/

generated $[Cu(dms)(dpa)]_n$, which showed a reduction in dimensionality from 3-D to 2-fold parallel interpenetrated (4,4) grids [12]. The longer-spanning dipyridyl ligand bis(4-pyridylmethyl)piperazine (4-bpmp) resulted in formation of $\{[Cu(suc)(4\text{-bpmp})(H_2O)_2]_n$, which possesses a 2D + 2D → 3D system of mutually inclined interpenetrated (4,4) grids [9c]. A self-penetrated 6-connected 4^86^68 **rob** lattice occurs in $\{[Cu_2(glu)_2(bpy)]\cdot 3H_2O\}_n$ [10a], in which the glu ligands rest in a *gauche-anti* conformation and construct $\{Cu_2(OCO)_4\}$ paddlewheel dimer-based $[Cu_2(glu)_2]_n$ layer motifs that are cross-pillared by bpy rigid-rod tethers. The longer 4-bpmp ligand afforded $\{[Cu_2(glu)_2(4\text{-bpmp})]\cdot 4H_2O\}_n$, which possessed an even less common self-penetrated 6-connected $4^46^{10}8$ **mab** topology [10b]. $[Cu_2(adp)_2(bpy)]_n$ displays a $\{Cu_2O_2\}$ dimer-based 2-fold interpenetrated $4^{12}6^3$ **pcu** network [11a]. $\{[Cu(adp)(H\text{-}4\text{-bpmp})(H_2O)]ClO_4\cdot 3H_2O\}_n$ displays $\{Cu_2O_2\}$ dimer-based (4,4) grid cationic layers with unligated perchlorate counterions [11b]. It is clear that the dipyridyl coligand, along with the aliphatic dicarboxylate component, plays a critical role in the self-selection of topological features during coordination polymer self-assembly.

In contrast to more heavily utilized dipyridyl ligands such as bpy, dpa, or 4-bpmp, the conformationally flexible dipyridylamide 3-pyridylmethylnicotinamide (3-pmna, Scheme 1) has not seen much use in the construction of coordination polymer solids [13]. Among the potential advantages of this ligand are its hydrogen bonding capability at central amide functional group, along with its ability to adopt *syn*, *anti*, or intermediate twisted conformations to facilitate different span lengths between adjacent metal centers in a putative coordination polymer. In this contribution we report the successful synthesis, structural and topological characterization, and preliminary physical property investigations of five new divalent copper coordination polymers containing aliphatic dicarboxylate ligands: $[Cu_2(suc)_2(3\text{-pmna})]_n$ (**1**), $\{[Cu_2(dms)_2(3\text{-pmna})]\cdot 4H_2O\}_n$ (**2**), $\{[Cu_2(glu)_2(3\text{-pmna})]\cdot H_2O\}_n$ (**3**), $[Cu(2\text{-mglu})(3\text{-pmna})]_n$ (**4**), and $\{[Cu_2(adp)_2(3\text{-pmna})_2]\cdot H_2O\}_n$ (**5**). We also report the structure of the minor product $\{[Cu_2(adp)_2(3\text{-pmna})]\cdot 0.25H_2O\}_n$ (**6**), formed during the synthesis of **5**.

2. Experimental

2.1. General considerations

Copper salts, dicarboxylic acids, and ligand synthesis precursors were purchased commercially. The 3-pmna ligand was prepared according to a modification a published procedure [14], employing 3-pyridylmethylamine and nicotinoyl chloride hydrochloride. Water was deionized above 3 MΩ-cm in-house. IR spectra were recorded on powdered samples using a Perkin Elmer Spectrum One instrument. Elemental Analysis was carried out using a Perkin Elmer 2400 Series II CHNS/O Analyzer. Thermogravimetric analysis was performed on a TA Instruments Q50 thermal analyzer under flowing N_2. Variable temperature magnetic susceptibility data (2–300 K) for **5** was collected on a Quantum Design MPMS SQUID magnetometer at an applied field of 0.1 T. After each temperature change the sample was kept at the new temperature for five minutes before magnetization measurement to ensure thermal equilibrium. The susceptibility data was corrected for diamagnetism using Pascal's constants [15], and also the diamagnetism of the polyethylene sample holder.

2.2. Preparation of $[Cu_2(suc)_2(3\text{-pmna})]_n$ (**1**)

$Cu(NO_3)_2\cdot 2.5H_2O$ (72 mg, 0.31 mmol), succinic acid (45 mg, 0.38 mmol) and 3-pmna (78 mg, 0.38 mmol) and 0.5 mL of a 1.0 M NaOH solution were placed into 10 mL distilled H_2O in a Teflon-lined acid digestion bomb. The bomb was sealed and heated in an oven at 120 °C for 24 h, and then cooled slowly to 25 °C. Green needles of 1 (26 mg, 24% yield based on Cu) were isolated after washing with distilled water and acetone, and drying in air. *Anal.* Calc. for $C_{20}H_{19}Cu_2N_3O_9$ **1**: C, 41.96; H, 3.35; N, 7.34. Found: C, 41.51; H, 3.34; N, 7.16%. IR (cm^{-1}): 3394 (w), 2979 (w), 1668 (w), 1616 (s), 1600 (s), 1533 (s), 1482 (w), 1428 (s), 1413 (w), 1398 (w), 1326 (m), 1297 (s), 1195 (w), 1180 (m), 1165 (w), 1130 (m), 1104 (w), 1052 (m), 1028 (m), 995 (m), 973 (m), 890 (w), 873 (m), 820 (m), 786 (w), 735 (m), 696 (s).

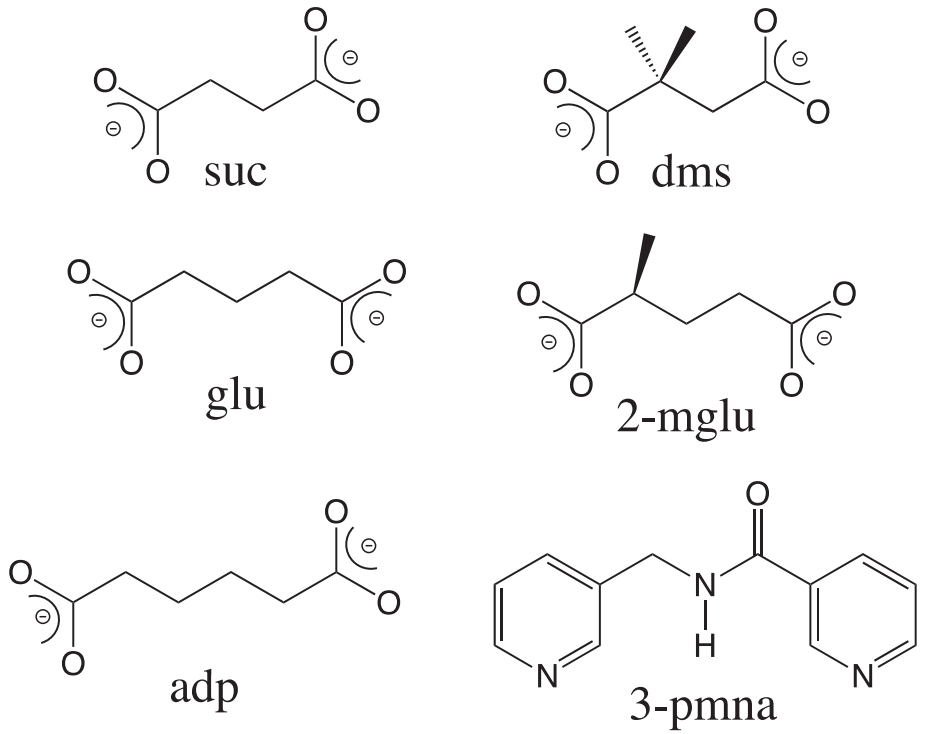

Scheme 1. Ligands used in this study.

2.3. Preparation of {[Cu_2(dms)$_2$(3-pmna)]·3.5H_2O}$_n$ (**2**)

$Cu(NO_3)_2$·2.5H_2O (72 mg, 0.31 mmol), 2,2-dimethylsuccinic acid (55 mg, 0.38 mmol) and 3-pmna (78 mg, 0.38 mmol) and 0.5 mL of a 1.0 M NaOH solution were placed into 10 mL distilled H_2O in a Teflon-lined acid digestion bomb. The bomb was sealed and heated in an oven at 120 °C for 24 h, and then cooled slowly to 25 °C. Green blocks of **2** (36 mg, 28% yield based on Cu) were isolated after washing with distilled water and acetone, and drying in air. *Anal.* Calc. for $C_{24}H_{35}Cu_2N_3O_{13}$ **2**: C, 41.14; H, 5.03; N, 6.00. Found: C, 41.71; H, 4.86; N, 6.15%. IR (cm^{-1}): 3308 (w), 1640 (sh), 1626 (s), 1599 (w), 1556 (w), 1474 (m), 1439 (s), 1373 (m), 1358 (w), 1305 (m), 1263 (m), 1223 (w), 1162 (w), 1135 (w), 1051 (w), 1029 (w), 893 (w), 828 (w), 785 (m), 708 (s), 668 (w).

2.4. Preparation of {[Cu_2(glu)$_2$(3-pmna)]·H_2O}$_n$ (**3**)

$CuSO_4$·5H_2O (86 mg, 0.37 mmol), glutaric acid (50 mg, 0.37 mmol) and 3-pmna (78 mg, 0.37 mmol) and 0.5 mL of a 1.0 M NaOH solution were placed into 10 mL distilled H_2O in a Teflon-lined acid digestion bomb. The bomb was sealed and heated in an oven at 120 °C for 24 h, and then cooled slowly to 25 °C. Green blocks of **3** (76 mg, 66% yield based on Cu) were isolated after washing with distilled water and acetone, and drying in air. *Anal.* Calc. for $C_{22}H_{25}Cu_2N_3O_{10}$ **3**: C, 42.72; H, 4.07; N, 6.79. Found: C, 42.74; H, 4.18; N, 6.76%. IR (cm^{-1}): 3471(w), 3236(w), 3082(2), 2978(w), 2938(w), 2258(w), 1644(m), 1610(m), 1599(w), 1597(m), 1480(m), 1461(m), 1444(w), 1430(m), 1403(s), 13 46(w), 1327(m), 1293(m), 1252(w), 1225(w), 1198(m), 1165(m), 1131(w), 1070(m), 1057(m), 1034(m), 985(w), 944(w), 879(w), 847(w), 830(w), 798(m), 761(w), 706(m), 682(w), 574(s).

2.5. Preparation of {[Cu(2-mglu)(3-pmna)]$_n$ (**4**)

$Cu(NO_3)_2$·2.5H_2O (72 mg, 0.31 mmol), 2-methylglutaric acid (55 mg, 0.37 mmol) and 3-pmna (78 mg, 0.37 mmol) and 0.75 mL of a 1.0 M NaOH solution were placed into 10 mL distilled H_2O in a Teflon-lined acid digestion bomb. The bomb was sealed and heated in an oven at 120 °C for 24 h, and then cooled slowly to 25 °C. Blue blocks of **4** (87 mg, 56% yield based on Cu) were isolated after washing with distilled water and acetone, and drying in air. *Anal.* Calc. for $C_{18}H_{19}CuN_3O_5$ **4**: C, 51.37; H, 4.55; N, 9.98. Found: C, 50.96; H, 4.62; N, 9.86%. IR (cm^{-1}): 3249(w), 1663(m), 1567(s), 1528(w), 1474(m), 1442(w), 1420(w), 1388(s), 1367(w), 1340(w), 1228(w), 1191(m), 1155(m), 1108(m), 1055(w), 1037(w), 969(w), 953(w), 845(w), 831(w), 817(m), 802(w), 773(w), 697(s), 657(s).

2.6. Preparation of {[Cu_2(adp)$_2$(3-pmna)$_2$]·H_2O}$_n$ (**5**) and {[Cu_2(adp)$_2$(3-pmna)]·0.25H_2O}$_n$ (**6**)

$CuSO_4$·5H_2O (86 mg, 0.37 mmol), sodium adipate (72 mg, 0.37 mmol) and 3-pmna (78 mg, 0.37 mmol) were placed into 10 mL distilled H_2O in a Teflon-lined acid digestion bomb. The bomb was sealed and heated in an oven at 120 °C for 24 h, and then cooled slowly to 25 °C. Blue crystals of **5** (97 mg, 61% yield based on Cu) were isolated after washing with distilled water and acetone, and drying in air. If the reaction was run at 150 °C, some green crystals of **6** were obtained in addition to blue crystals of **5**. Manual separation of bulk quantities of **6** was not practical. *Anal.* Calc. for $C_{36}H_{40}Cu_2N_6O_{11}$ **5**: C, 50.29; H, 4.69; N, 9.77. Found: C, 49.65; H, 4.69; N, 9.62%. IR (cm^{-1}): 3544 (w), 3406 (w), 3221 (w) 3066 (w), 2958 (w) 2800 (w), 1659 (m), 1638 (w),1602 (m), 1566 (s), 1537 (s), 1479 (m) 1463 (w) 1428 (m),1379 (s), 1360 (m), 1329 (w), 1314 (m), 1266 (w), 1223 (w) 1210 (w), 1198 (m), 1159 (m), 1133 (w), 1115 (w), 1110 (w), 1084 (w),1059 (w), 1038 (w), 1029 (w), 989 (m), 928 (m), 917 (w), 830 (m), 810 (m),796 (m), 784 (m), 757 (w), 695 (s), 665 (m), 655 (s).

3. X-ray crystallography

Single crystal X-ray diffraction was performed on single crystals of **1**–**6** with a Bruker-AXS ApexII CCD instrument at 173 K, with the exception of **1**, whose data was collected at 293 K. Reflection data were acquired using graphite–monochromated Mo Kα radiation (λ = 0.71073 Å), with the exception for **2**, which was acquired using Cu Kα radiation (λ = 1.54178 Å). The data was integrated via SAINT [16]. Lorentz and polarization effect and empirical absorption corrections were applied with SADABS [17]. The structures were solved using direct methods and refined on F^2 using SHELXTL [18] subroutines within the OLEX2 crystallographic suite [19]. All non-hydrogen atoms were refined anisotropically. Hydrogen atoms were placed in calculated positions and refined isotropically with a riding model. The crystal of **1** exhibited a small needle morphology and proved to be a triple twin according to CELL NOW [20]. Only data from the major twin component was used in the solution and refinement. As a result of the small crystal size, twinning, and relatively weak intensity, the data set for **1** is somewhat incomplete (93.8% to a 2Θ of 50°) with a high R_{int} value. The molecular connectivity proved to be unambiguous and thermal displacement parameters refined acceptably. Two different orientations of the 3-pmna ligand in the crystal structure of **2** were successfully modeled using partial occupancies. Some significant disorder across the crystallographic mirror plane was present in the 3-pmna ligand in **3**. Attempts at solving the structures for **2**, **4** and **5** in centrosymmetric space groups did not yield acceptable solutions or refinements. The crystal of **2** was refined as a perfect inversion twin. The Flack parameters [21] for **4** and **5** are 0.00(16) and −0.02(2), indicating relatively high enantiomeric purity within the respective single crystals. Relevant crystallographic data for **1**–**6** is listed in Table 1.

4. Results and discussion

4.1. Synthesis and infrared spectra

Compounds **1**–**5** were prepared cleanly by hydrothermal reaction of divalent copper salts with the requisite aliphatic dicarboxylic acid and 3-pyridylmethylnicotinamide. Compound **6** was obtained as a minor product during a higher temperature attempt to optimize the yield of compound **5**. The infrared spectra of compounds **1**–**5** were consistent with structural components determined by single-crystal X-ray diffraction. Intense, slightly broadened asymmetric and symmetric C–O stretching bands were observed at 1616 and 1428 cm^{-1} in **1**, 1626 and 1439 cm^{-1} in **2**, 1610 and 1403 cm^{-1} in **3**, 1567 and 1388 cm^{-1} in **4**, and 1566 and 1379 cm^{-1} in **5**. Sharper bands in the range of ~1610 to ~1300 cm^{-1} were attributed to stretching modes of pyridyl rings of nitrogen base ligands [22]. Features corresponding to C–H bending and arene puckering within the pyridyl rings exist in the region between ~900 and ~650 cm^{-1}. The C=O stretching bands within the 3-pmna ligands were observed at 1668 cm^{-1} in **1**, 1640 cm^{-1} in **2**, 1644 cm^{-1} in **3**, 1663 cm^{-1} in **4**, and 1659 cm^{-1} in **5**. Broad, weak spectral bands in the vicinity of ~3000–3200 cm^{-1} indicate the presence of any 3-pnma N–H bonds and unbound water molecules where present.

4.2. Structural description of [Cu_2(suc)$_2$(3-pmna)]$_n$ (**1**)

The asymmetric unit of compound **1** contains two divalent copper atoms (Cu1, Cu2), two suc ligands (suc-A, suc-B), and one 3-

Table 1
Crystal and structure refinement data for **1–6**.

Data	**1**	**2**	**3**	**4**	**5**	**6**
Empirical Formula	$C_{20}H_{19}Cu_2N_3O_9$	$C_{24}H_{35}Cu_2N_3O_{13}$	$C_{22}H_{25}Cu_2N_3O_{10}$	$C_{18}H_{19}CuN_3O_5$	$C_{36}H_{40}Cu_2N_6O_{11}$	$C_{24}H_{27.5}Cu_2N_3O_{9.25}$
Formula weight	572.46	700.63	618.53	420.90	859.82	633.07
Crystal system	triclinic	triclinic	monoclinic	orthorhombic	monoclinic	monoclinic
Space group	$P\bar{1}$	$P1$	$P2_1/m$	$Fdd2$	$P2_1$	$C2/c$
a (Å)	6.646(2)	6.1938(3)	7.1482(17)	32.610(7)	11.488(3)	34.701(13)
b (Å)	10.451(6)	10.8349(6)	17.056(4)	43.566(10)	9.184(3)	8.354(3)
c (Å)	15.661(9)	12.6042(7)	10.403(2)	4.8769(11)	16.993(5)	22.244(9)
α (°)	105.483(6)	111.131(3)	90	90	90	90
β (°)	92.571(7)	95.920(3)	106.655(7)	90	99.116(4)	125.783(13)
γ (°)	101.665(7)	103.552(3)	90	90	90	90
V (Å^3)	1021.0(10)	750.41(7)	1215.1(5)	6929(3)	1770.3(9)	5231(3)
Z	2	1	2	16	2	8
D_{calc} (g cm^{-3})	1.862	1.550	1.691	1.614	1.613	1.608
μ (mm^{-1})	2.145	2.344	1.813	1.298	1.274	1.684
Minimum/ maximum trans.	0.64	0.8369	0.8756	0.810	0.739	0.917
hkl ranges	$-7 \leqslant h \leqslant 7$, $-12 \leqslant k \leqslant 11$, $0 \leqslant l \leqslant 18$	$-7 \leqslant h \leqslant 7$, $-12 \leqslant k \leqslant 13$, $-15 \leqslant l \leqslant 15$	$-8 \leqslant h \leqslant 8$, $-20 \leqslant k \leqslant 20$, $-12 \leqslant l \leqslant 12$	$-38 \leqslant h \leqslant 0$, $-51 \leqslant k \leqslant 3$, $-5 \leqslant l \leqslant 5$	$-13 \leqslant h \leqslant 13$, $-11 \leqslant k \leqslant 10$, $-20 \leqslant l \leqslant 20$	$-41 \leqslant h \leqslant 41$, $-9 \leqslant k \leqslant 9$, $-26 \leqslant l \leqslant 26$
Total reflections	18450	11057	9958	27964	14733	40762
Unique reflections	3436	4613	2299	2860	5928	4685
R_{int}	0.1942	0.0537	0.0693	0.1052	0.1038	0.1016
Parameters	295	392	193	246	499	346
R_1 (all data)[a]	0.2067	0.0525	0.0573	0.0844	0.1127	0.0755
R_1 [$I > 2\sigma(I)$][a]	0.0837	0.0447	0.0391	0.0582	0.0708	0.0442
wR_2 (all data)[b]	0.1896	0.1286	0.0897	0.1390	0.1852	0.1154
wR_2 [$I > 2\sigma(I)$][b]	0.1574	0.1196	0.0858	0.1297	0.1595	0.0994
Maximum/ minimum residual (e Å^{-3})	0.768/–0.795	0.859/–0.398	0.662/–0.717	0.788/–0.476	1.575/–0.829	0.980/–0.392
Goodness-of-fit (GOF)	0.925	1.062	1.174	1.077	1.001	1.024

[a] $R_1 = \sum||F_o| - |F_c||/\sum|F_o|$.
[b] $wR_2 = \{\sum[w(F_o^2 - F_c^2)^2]/\sum[wF_o^2]^2\}^{1/2}$.

pmna ligand. Both of the crystallographically distinct copper atoms show very slightly distorted {CuO_4N} square pyramidal coordination environments (Fig. 1a), with Addison τ values [23] of 0.002 and 0.011 for Cu1 and Cu2, respectively. The basal plane of the Cu1 square pyramid contains oxygen donor atoms from four different suc-A ligands, while that of Cu2 contains oxygen donor atoms from four different suc-B ligands. In the apical position at Cu1 is situated a nicotinamide nitrogen atom donor from a 3-pmna ligand, while that at Cu2 is occupied by a 3-pyridylmethyl nitrogen donor atom from the same 3-pmna ligand. Bond lengths and angles within the coordination spheres in **1** are listed in Table 2.

Both the suc-A and suc-B ligands in **1** adopt a μ_4-κ^4-O:O′:O″:O‴ binding mode, with *syn–syn* carboxylate bridges at each terminus connecting pairs of copper atoms. As result, standard paddlewheel {$Cu_2(OCO)_4$} dimeric units are formed, between pairs of Cu1 atoms or between pairs of Cu2 atoms. The Cu1···Cu1 distance provided by the bridging carboxylate groups of the suc-A ligands measures 2.663(3) Å; the related distance between Cu2 atoms linked by suc-B carboxylate groups is 2.649(3) Å. All of the suc ligands man-

Table 2
Selected bond distance (Å) and angle (°) data for **1**.

Cu1–O1	1.974(7)	Cu2–O5$^{\#4}$	1.974(8)
Cu1–O2$^{\#1}$	2.003(8)	Cu2–O6$^{\#5}$	1.987(7)
Cu1–O3$^{\#2}$	1.958(8)	Cu2–O7$^{\#2}$	1.999(8)
Cu1–O4$^{\#3}$	1.965(8)	Cu2–O8	1.960(7)
Cu1–N1	2.197(9)	Cu2–N3	2.156(9)
O1–Cu1–O2$^{\#1}$	167.2(3)	O5$^{\#4}$–Cu2–O6$^{\#5}$	88.8(3)
O1–Cu1–N1	109.6(4)	O5$^{\#4}$–Cu2–O7$^{\#2}$	167.9(3)
O2$^{\#1}$–Cu1–N1	83.0(4)	O5$^{\#4}$–Cu2–N3	101.0(3)
O3$^{\#2}$–Cu1–O1	89.8(3)	O6$^{\#5}$–Cu2–O7$^{\#2}$	90.8(3)
O3$^{\#2}$–Cu1–O2$^{\#1}$	87.8(3)	O6$^{\#5}$–Cu2–N3	97.5(3)
O3$^{\#2}$–Cu1–O4$^{\#3}$	167.1(3)	O7$^{\#2}$–Cu2–N3	91.1(3)
O3$^{\#2}$–Cu1–N1	92.6(4)	O8–Cu2–O5$^{\#4}$	88.8(3)
O4$^{\#3}$–Cu1–O1	89.0(3)	O8–Cu2–O6$^{\#5}$	167.2(3)
O4$^{\#3}$–Cu1–O2$^{\#1}$	90.5(3)	O8–Cu2–O7$^{\#2}$	88.9(3)
O4$^{\#3}$–Cu1–N1	99.9(4)	O8–Cu2–N3	95.3(3)

Symmetry transformations to generate equivalent atoms: #1 $-x+1, -y, -z+2$; #2 $x-1, y, z$; #3 $-x+2, -y, -z+2$; #4 $-x+1, -y, -z+1$; #5 $-x, -y, -z+1$.

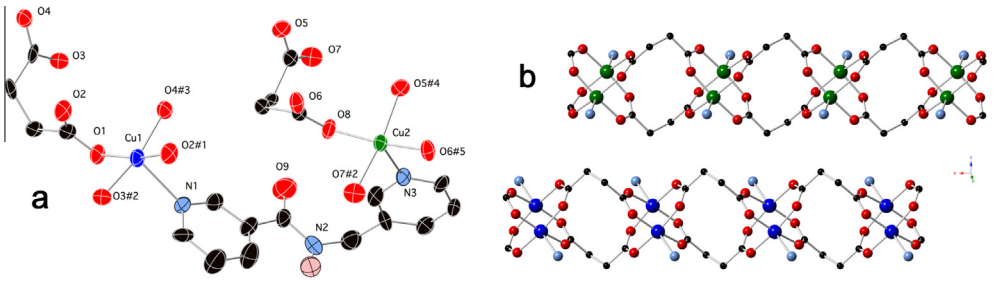

Fig. 1. (a) Coordination environment in **1**. (b) $[Cu_2(suc)_2]_n$ chain submotifs in **1** with embedded {$Cu_2(OCO)_4$} paddlewheel dimers.

ifest a *gauche* conformation, with torsion angles of 77.3° and 71.3° for suc-A and suc-B, respectively. The aliphatic chains of the suc ligands link neighboring $\{Cu_2(OCO)_4\}$ dimeric units into $[Cu_2(suc)_2]_n$ 1-D chain motifs (Fig. 1b). The interdimer Cu···Cu distances spanned by either the suc-A or suc-B ligands measure 6.646 Å, marking the *a* lattice parameter.

Neighboring $[Cu_2(suc)_2]_n$ chains are connected into $[Cu_2(suc)_2(3\text{-pmna})]_n$ coordination polymer layers (Fig. 2a) by *syn*-conformation 3-pmna ligands (N···C_{arom}···C_{arom}···N torsion angle = 27.8°), that span a Cu···Cu distance of 8.214 Å. A side view of a single layer motif (Fig. 2b), oriented parallel to the *ac* crystal plane, reveals a distinct undulation imparted by the curled conformation of the 3-pmna ligands bridging copper atoms in adjacent chain submotifs. Considering the $\{Cu_2(OCO)_4\}$ dimers as connecting nodes, with 3-pmna ligands and *gauche* suc ligand pairs treated as linkers, reveals an underlying (4,4) grid topology for the coordination polymer layers in **1**. Individual $[Cu_2(suc)_2(3\text{-pmna})]_n$ layers stack and interdigitate along the *b* crystal direction (Fig. S1) via π–π supramolecular interactions between pyridyl rings of nearby 3-pmna ligands (centroid-to-centroid distances = 3.545(7) and 3.786(8) Å). There is no solvent accessible space between adjacent layers for the occlusion of any co-crystallized species.

4.3. Structural description of $\{[Cu_2(dms)_2(3\text{-pmna})]\cdot 4H_2O\}_n$ (**2**)

Compound **2** crystallized in the non-centrosymmetric triclinic space group with an asymmetric unit containing two divalent copper atoms, two dms ligands, one 3-pmna ligand fully disordered in a 50/50 ratio over two sets of positions, and net four water molecules of crystallization across several disordered positions. The coordination environments at the crystallographically distinct copper atoms were both $\{CuO_4N\}$ square pyramids (τ = 0.015 and 0.013, Fig. 3a), with the basal positions taken up by oxygen atom donors from four dms ligands. The Jahn–Teller elongated apical position is occupied by a nitrogen donor atom from a 3-pmna ligand. According to the disorder model, the pyridylmethylamine and nicotinamide pyridyl rings supply this donor in a 50/50 ratio of possibilities. Bond lengths and angles within the coordination spheres are listed in Table 3.

All of the dms ligands in **2** adopt a μ_4-κ^4-O:O′:O″:O‴ binding mode, with *syn–syn* carboxylate bridges at each terminus. Via these dms bridging modes, standard paddlewheel $\{Cu_2(OCO)_4\}$ dimers are constructed, with a Cu···Cu distance of 2.625 Å. The full span of the dms ligands links the dimeric units into $[Cu_2(dms)_2]_n$ 1-D chain motifs (Fig. 3b), with the closest interdimer Cu···Cu distance measuring 6.198 Å. In turn these chains are connected into $[Cu_2(dms)_2(3\text{-pmna})]_n$ coordination polymer layers (Fig. 3c) by tethering *anti*-conformation 3-pmna ligands (N···C_{arom}···C_{arom}···N torsion angle = 115°), with a Cu···Cu distance of 13.011 Å. Treating the $\{Cu_2(OCO)_4\}$ dimers as a connecting node reveals an underlying (4,4) grid topology for **2**.

Individual $[Cu_2(dms)_2(3\text{-pmna})]_n$ coordination polymer layers are oriented parallel to the $[0\bar{1}1]$ crystal planes, and stack in an AAA pattern along the *b* crystal direction (Fig. S2). The steric bulk of the methyl groups of the dms ligands prevents the close layer stacking and π–π interactions evident in the unsubstituted succinate derivative **1**. The disordered water molecules of crystallization are anchored to the coordination polymer layers by hydrogen bonding patterns involving the amide functional groups of the 3-pmna ligands. These provide the supramolecular interactions necessary for aggregation of the layer motifs. The disordered water molecules occupy solvent-accessible regions comprising 13.7% of the unit cell volume according to PLATON [24].

4.4. Structural description of $\{[Cu_2(glu)_2(3\text{-pmna})]\cdot H_2O\}_n$ (**3**)

Compound **3** crystallized in a centrosymmetric monoclinic space group with an asymmetric unit containing a divalent copper atom, halves of two glu ligands, a half-occupied water molecule of crystallization, and one-half of a 3-pmna ligand disordered across a crystallographic mirror plane. In a very similar fashion to **1** and **2**, the copper atom displays a $\{CuO_4N\}$ square pyramidal (τ = 0.001) coordination environment (Fig. 4a), with the basal positions filled by oxygen atom donors from four glu ligands. Again, the elongated apical position is occupied by a nitrogen donor atom from a 3-pmna ligand. Bond lengths and angles within the coordination environment are listed in Table 4.

The *anti-anti* conformation glu ligands in **3** (torsion angles = 170.1° or 178.4°) display the same μ_4-κ^4-O:O′:O″:O‴ binding mode as the dms ligands in **1** and **2** with exobidentate *syn–syn* carboxylate bridges at each terminus. Similar $\{Cu_2(OCO)_4\}$ paddlewheel dimers are constructed as those in **1**, with an identical Cu···Cu distance of 2.625 Å. $[Cu_2(glu)_2]_n$ 1-D chain motifs are seen in **3**, similar to the $[Cu_2(suc)_2]_n$ chains in **1** and the $[Cu_2(dms)_2]_n$ chains in **2**. However in great contrast to **2**, the 3-pmna ligands in **3** manifest a symmetry restricted *syn* conformation

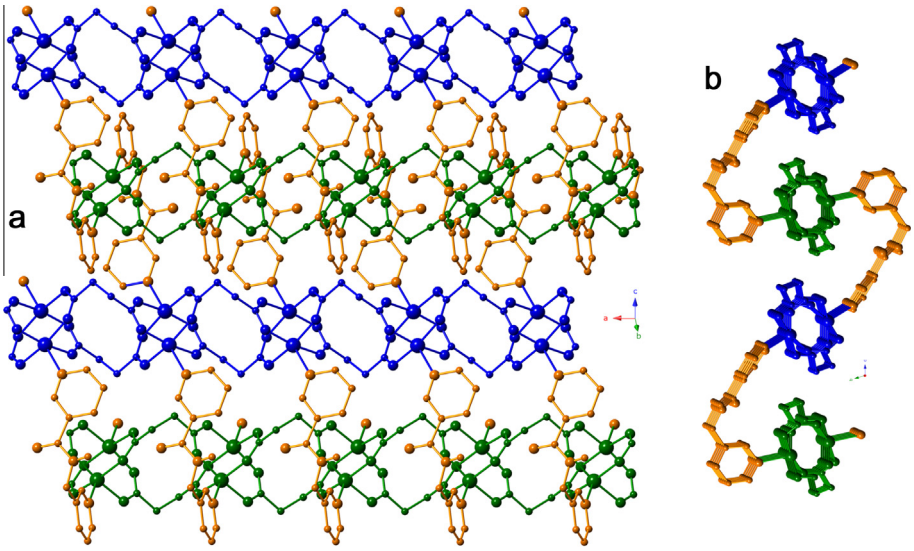

Fig. 2. $[Cu_2(suc)_2(3\text{-pmna})]_n$ layer in **1**. (a) Face view and (b) Side view.

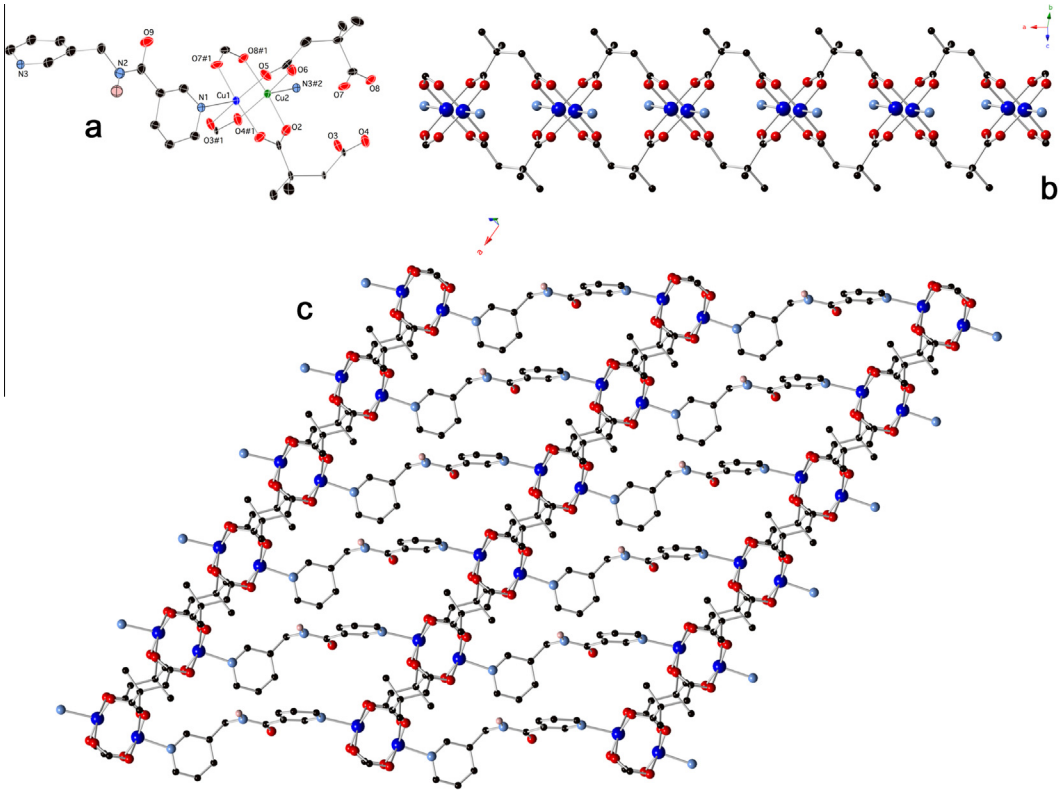

Fig. 3. (a) Coordination environments in **2**, with only one 3-pmna disorder component shown. (b) $[Cu_2(dms)_2]_n$ chain submotif in **2** with embedded $\{Cu_2(OCO)_4\}$ paddlewheel dimers. (c) $[Cu_2(dms)_2(3\text{-pmna})]_n$ layer in **2**.

Table 3
Selected bond distance (Å) and angle (°) data for **2**.

Cu1–O1	1.976(9)	Cu2–O2	1.951(9)
Cu1–O3$^{\#1}$	1.990(8)	Cu2–O4$^{\#1}$	1.987(8)
Cu1–O5	1.987(8)	Cu2–O6	1.953(9)
Cu1–O7$^{\#1}$	1.940(8)	Cu2–O8$^{\#1}$	1.957(8)
Cu1–N1	2.256(17)	Cu2–N3$^{\#2}$	2.11(2)
O1–Cu1–O3$^{\#1}$	88.4(4)	O2–Cu2–O4$^{\#1}$	87.4(4)
O1–Cu1–O5	92.6(4)	O2–Cu2–O6	91.3(4)
O1–Cu1–N1	99.0(4)	O2–Cu2–O8$^{\#1}$	168.1(4)
O3$^{\#1}$–Cu1–N1	88.0(6)	O2–Cu2–N3$^{\#2}$	94.7(7)
O5–Cu1–O3$^{\#1}$	168.1(3)	O4$^{\#1}$–Cu2–N3	97.1(5)
O5–Cu1–N1	103.5(6)	O6–Cu2–O4$^{\#1}$	168.9(4)
O7$^{\#1}$–Cu1–O1	169.0(4)	O6–Cu2–O8$^{\#1}$	87.1(4)
O7$^{\#1}$–Cu1–O3$^{\#1}$	89.0(4)	O6–Cu2–N3$^{\#2}$	94.0(6)
O7$^{\#1}$–Cu1–O5	87.8(4)	O8$^{\#1}$–Cu2–O4$^{\#1}$	91.9(4)
O7$^{\#1}$–Cu1–N1	91.6(5)	O8$^{\#1}$–Cu2–N3$^{\#2}$	97.2(6)

Symmetry transformations to generate equivalent atoms: #1 $x, y, z+1$; #2 $x-2$; $y-1, z-1$.

Table 4
Selected bond distance (Å) and angle (°) data for **3**.

Cu1–O1$^{\#1}$	1.972(2)	O1$^{\#1}$–Cu1–N2	96.45(10)
Cu1–O2	1.975(2)	O2–Cu1–O3	88.67(10)
Cu1–O3	1.980(2)	O2–Cu1–N2	94.88(11)
Cu1–O4$^{\#1}$	1.978(2)	O3–Cu1–N2	99.42(10)
Cu1–N2	2.158(3)	O4$^{\#1}$–Cu1–O2	90.83(11)
O1$^{\#1}$–Cu1–O2	168.65(10)	O4$^{\#1}$–Cu1–O3	168.72(10)
O1$^{\#1}$–Cu1–O3	88.91(10)	O4$^{\#1}$–Cu1–N2	91.86(10)
O1$^{\#1}$–Cu1–O4$^{\#1}$	89.38(11)		

Symmetry transformation to generate equivalent atoms: #1 $-x, -y+1, -z$.

(N···C_{arom}···C_{arom}···N torsion angle = 0°), allowing them to bridge between copper atoms within the same chain motif. The *syn*-conformation 3-pmna ligands in **3** span a Cu···Cu distance of 8.104 Å, almost 3 Å shorter than the *anti*-conformation 3-pmna ligands in **2**. This distance corresponds exactly to the closest interdimer Cu···Cu contact mediated by the glu ligands within the resulting 1-D $[Cu_2(glu)_2(3\text{-pmna})]_n$ ribbon motifs (Fig. 4b). The longer Cu···Cu interdimer contact bridged by the glu ligands, which measures 8.952 Å, is too long to be bridged the *syn* conformation 3-pmna ligands.

As a result of the longer Cu···Cu dicarboxylate distance and the shorter Cu···Cu distance through the conformationally flexible

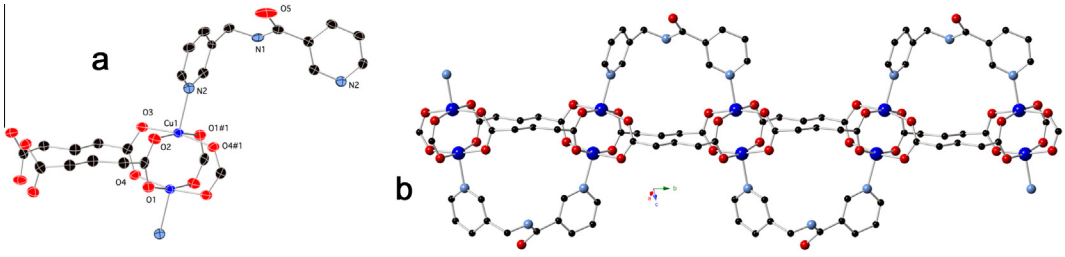

Fig. 4. (a) Coordination environment in **3**. Only one of the disordered 3-pmna conformations is depicted. (b) $\{[Cu_2(glu)_2(3\text{-pmna})]_n$ chain motif in **3** with embedded $\{Cu_2(OCO)_4\}$ paddlewheel dimers and curled conformation 3-pmna ligands.

3-pmna ligand, a 2-D layer motif is prevented in **3**. Neighboring $[Cu_2(glu)_2(3\text{-pmna})]_n$ ribbons are arranged parallel to the *b* crystal direction, and engage in π–π stacking via the pyridyl rings of 3-pmna ligands to construct supramolecular layers (Fig. S3). Isolated water molecules of crystallization in **3** are contained in very small solvent-accessible regions between these pseudolayers comprising 2.4% of the unit cell volume. They are anchored to the coordination polymer ribbons by donating hydrogen bonds to 3-pmna amide oxygen atoms and ligated glu carboxylate oxygen atoms (Table S1), and in turn provide the impetus for aggregation of the supramolecular layer motifs (Fig. S4).

Table 5
Selected bond distance (Å) and angle (°) data for **4**.

Cu1–O3$^{\#1}$	1.948(5)	O5–Cu1–O3$^{\#1}$	176.4(2)
Cu1–O5	1.938(5)	O5–Cu1–N1	93.4(2)
Cu1–N1	1.984(6)	O5–Cu1–O4$^{\#2}$	94.83(19)
Cu1–O4$^{\#2}$	2.228(5)	O5–Cu1–N3$^{\#1}$	89.3(2)
Cu1–N3$^{\#1}$	2.054(6)	N1–Cu1–O4$^{\#2}$	95.5(2)
O3$^{\#1}$–Cu1–N1	86.1(2)	N1–Cu1–N3$^{\#1}$	174.7(2)
O3$^{\#1}$–Cu1–O4$^{\#2}$	88.7(2)	N3$^{\#1}$–Cu1–O4$^{\#2}$	88.8(2)
O3$^{\#1}$–Cu1–N3$^{\#1}$	90.9(2)		

Symmetry transformations to generate equivalent atoms: #1 $x-1/4$, $-y+1/4$; $-z+3/4$; #2 x, y, $z+1$.

4.5. Structural description of $[Cu(2\text{-mglu})(3\text{-pmna})]_n$ (**4**)

Compound **4** crystallized as a racemic twin in the acentric orthorhombic space group *Fdd*2 with a simple asymmetric unit containing a divalent copper atom, a fully deprotonated 2-mglu ligand, and a 3-pmna ligand. The copper atom displays a very slightly distorted $\{CuO_3N_2\}$ square pyramidal ($\tau = 0.03$) coordination environment (Fig. 5a), with carboxylate oxygen atom donors from three 2-mglu ligands in trans basal positions and in the apical site. Pyridyl nitrogen atom donors from two 3-pmna ligands take up the remaining two trans basal positions. Bond lengths and angles within the coordination environment are listed in Table 5.

Unlike the exotetradentate glu ligands in **3**, the 2-mglu ligands in **4** adopt an exotridentate μ_3-κ^3-O:O′:O″ binding mode. One carboxylate terminus bridges two copper atoms in an *anti-syn* fashion between their basal and apical coordination sites, constructing 1-D $\{CuOCO\}_n$ chain submotifs with a Cu···Cu distance of 4.877 Å defining the tight *c* lattice parameter. The full span of the *gauche-anti* conformation (torsion angles = 60.3°, 175.4°) glutarate chain of the 2-mglu ligands links the 1-D $\{CuOCO\}_n$ chains into $[Cu(2\text{-mglu})]_n$ 2-D coordination polymer layer patterns (Fig. 5b). The through-ligand distance across the 2-mglu ligand is 9.229 Å. This same distance is spanned by curled *syn*-conformation 3-pmna ligands (N···C_{arom}···C_{arom}···N torsion angle = 21.6°), resulting in a $[Cu(2\text{-mglu})(3\text{-pmna})]_n$ coordination polymer layer, viewed from an face-on perspective in Fig. 6a. A edge-on perspective (Fig. 6b) reveals significant undulations within the $[Cu(2\text{-mglu})(3\text{-pmna})]_n$ layer motif.

The topology of **4** was investigated by considering the exotridentate 2-mglu ligands as 3-connected nodes and the copper atoms themselves as 5-connected nodes. A calculation performed via TOPOS [25] revealed a topology with a point symbol of $(3.5^2)(3^2.5^3.6^4.7)$, with net classification 3,5L52 (Fig. 6c). This net is not very common in coordination polymer chemistry, among the few reports is the underlying topology of $\{[Co_2(3,3',4,4'\text{-oxidiphthalate})(bbi)]\cdot 3H_2O\}_n$ (bbi = 1,1′-(1,4-butanediyl)bis(imidazole)) [26]. Layer motifs in **4** stack in an *ABCD* pattern along the *b* crystal axis, related by crystallographic glide planes (Fig. S5). Non-classical C–H···O supramolecular interactions (C···O distance = 3.448(9) Å) serve to aggregate neighboring layers, between the methylene group of 3-pmna ligands in one layer and the carbonyl oxygen atom of other 3-pmna ligands in another layer. The increase in dimensionality of the 2-methylglutarate derivative **4** from its unsubstituted congener **3** runs counter to previously recognized trends in coordination polymer structural chemistry [27].

4.6. Structural description of $\{[Cu_2(adp)_2(3\text{-pmna})_2]\cdot H_2O\}_n$ (**5**)

The asymmetric unit of compound **5** contains two crystallographically distinct copper atoms (Cu1, Cu2), two adp ligands (adp-A, adp-B), two 3-pmna ligands, and a water molecule of crystallization. Both Cu1 and Cu2 atoms display distorted $\{CuO_3N_2\}$ square pyramidal coordination environments (Fig. 7a), with τ values equaling 0.165 and 0.195, respectively. The basal plane of the square pyramid at Cu1 contains two trans 3-pmna pyridyl nitrogen donor atoms, an oxygen donor from adp-A, and an oxygen donor from adp-B, with the apical site filled by an oxygen donor atom from a second adp-A ligand. The basal plane at Cu2 is filled with the same type of donors as that of Cu1, while its apical site is occupied by an oxygen donor atom from a second adp-B ligand. Bond lengths and angles within the coordination environments in **5** are listed in Table 6.

Crystallographic distinction between the adp ligands is brought about by conformational differences. The adp-A ligands adopt an *anti-anti-anti* conformation with four C-atom torsion angles of 169.4, 170.9, and 177.5°. Meanwhile the adp-B ligands have a more curled *anti-gauche-anti* conformation with related torsion angles of 175.0, 52.3, and 161.4°. Both do manifest an exotridentate μ_3-κ^3-O:O′:O″ binding mode, with adp-A ligands bridging two Cu1 atoms and one Cu2 atom, and the adp-B ligands bridging two Cu2 atoms and one Cu1 atom. The Cu1 atoms are bridged by carboxylate groups of the adp-A ligands in *anti-syn* manner, connecting an apical site on one Cu1 atom to a basal site on another Cu1 atom. The Cu1 atoms thus are linked into $[(Cu1)(OCO)]_n$ chain motifs oriented parallel to the *b* crystal direction, with a Cu···Cu distance of 5.019 Å. Similarly, the Cu2 atoms are bridged by carboxylate

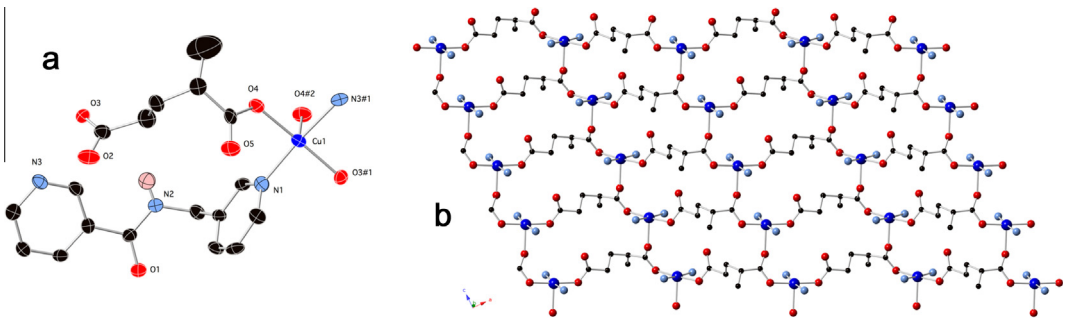

Fig. 5. (a) Coordination environment in **4** and (b) $[Cu(2\text{-mglu})]_n$ layer submotif in **4** with *anti-syn* bridged $\{CuOCO\}_n$ chains.

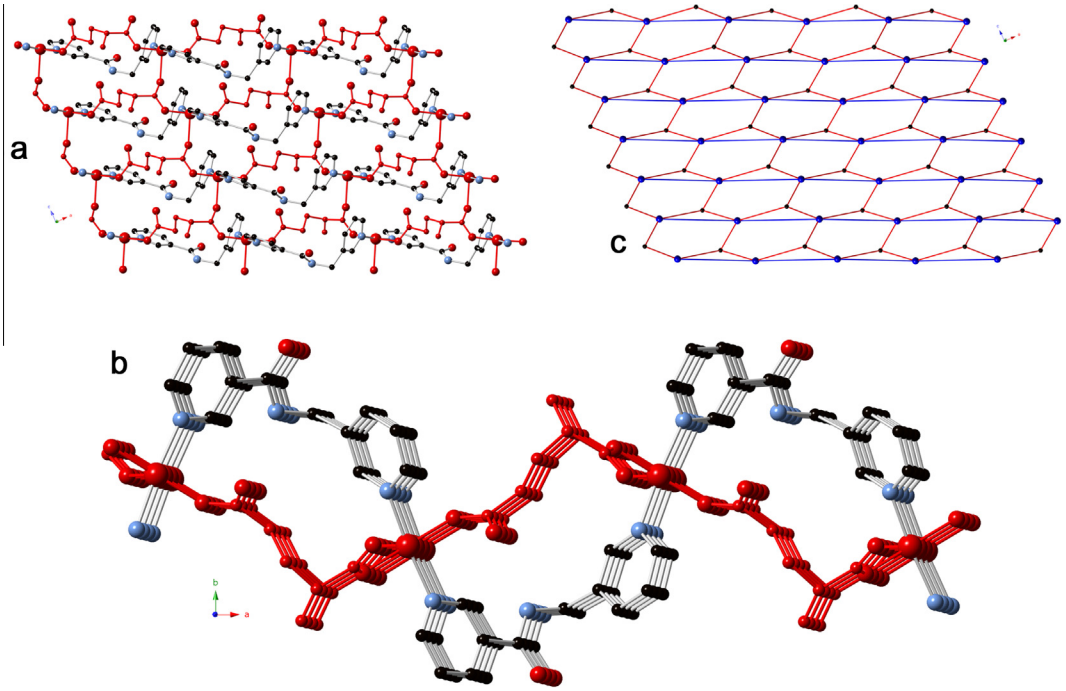

Fig. 6. (a) Face-on on view of the $[Cu(2\text{-mglu})(3\text{-pmna})]_n$ layer in **4**, with $[Cu(2\text{-mglu})]_n$ layer submotif drawn in red in the online version of this article. (b) Edge-on on view of the $[Cu(2\text{-mglu})(3\text{-pmna})]_n$ layer in **4**. (c) Schematic perspective of 3,5-connected $(3.5^2)(3^25^36^47)$ 2-D topology of **4**. The 5-connected copper atoms and the 3-connected 2-mglu ligand nodes are shown as larger and smaller spheres, respectively. (For interpretation of the references to colour in this figure legend, the reader is referred to the web version of this article.)

groups of the adp-B ligands in *anti-syn* apical-basal fashion. These linkages construct $[(Cu2)(OCO)]_n$ chain patterns, also arranged parallel to the *b* crystal direction. The Cu···Cu distance between the carboxylate-bridged Cu2 atoms is shorter, measuring 4.826 Å. The full span of the adp ligands connect Cu1 atoms to Cu2 atoms; the Cu···Cu distances through adp-A and adp-B ligands are 11.260 Å and 10.796 Å, respectively. The shorter distance through the adp-B ligands is caused by its more curled *anti-gauche-anti* conformation, when compared to the *anti-anti-anti* conformation of adp-A. Through these interactions, $[Cu_2(adp)_2]_n$ coordination polymer layer motifs are formed (Fig. 7b). As the Cu atoms and exotridentate adp ligands both serve as 3-connected nodes, the overall topology of the $[Cu_2(adp)_2]_n$ motifs is that of a simple graphitic (6,3) net.

Neighboring $[Cu_2(adp)_2]_n$ layers are connected into a 3-D $[Cu_2(adp)_2(3\text{-pmna})_2]_n$ coordination polymer network by tethering 3-pmna ligands (Fig. 8a). These span Cu···Cu distances of 11.488 Å, which denotes the *a* lattice parameter. The crystallographically distinct 3-pmna ligands adopt a twisted *anti*-conformation (N···C_{arom}···C_{arom}···N torsion angles = 127.8° and 132.5°). Treating the 3-pmna ligands as simple connectors, the overall topology of **5** was determined to be a non-interpenetrated 3,5-connected **hms** net (Fig. 8b), with a point symbol of $(6^3)(6^98)$. Only one other **hms** net has been reported previously with metal atoms serving as 5-connected nodes and exotridentate carboxylate-type ligands serving as 3-connected nodes, seen in $[Ni(Hbtc)(bpy)\cdot 3DMF]_n$ (btc = 1,3,5-benzenetricarboxylate) [28]. The coordination polymer net of **5** is stabilized by hydrogen bonding donation from the 3-pmna amide groups to the unligated adp-A and adp-B carboxylate oxygen atoms. Isolated water molecules of crystallization are located in small pockets comprising 2.0% of the unit cell volume, held to the coordination polymer framework by donating hydrogen bonds to 3-pmna carbonyl groups and to ligated adp-B carboxylate oxygen atoms.

4.7. Structural description of $\{[Cu_2(adp)_2(3\text{-pmna})]\cdot 0.25H_2O\}_n$ (**6**)

The asymmetric unit of compound **6** contains two divalent copper atoms (Cu1, Cu2), two adp ligands (adp-A, adp-B), a 3-pmna ligand, and an unligated water molecule best refined at 25% occupancy. Both of the crystallographically distinct copper atoms in **6** show $\{CuO_4N\}$ square pyramidal coordination environments (Fig. 9a), with τ values of 0.005 and 0.001, respectively. At both Cu1 and Cu2, trans oxygen atom donors from two adp-A ligands and trans oxygen atom donors from two adp-B ligands fill the basal planes. The pyridyl nitrogen donor atom bound in the apical position at Cu1 belongs to a pyridylmethyl group of a 3-pmna ligand, while the pyridyl nitrogen donor atom in the apical site at Cu2 belongs to a nicotinamide group of another 3-pmna ligand. Bond lengths and angles within the square pyramidal coordination environments are listed in Table 7.

Both the adp-A and adp-B ligands in **6** adopt different *anti-anti-gauche* conformations, different from the adp ligands in **5**. The adp-A ligands show four C-atom torsion angles of 165.0, 174.4, and 70.1°, while the related values for the adp-B ligands are 179.2, 175.0, and 74.2°. Both also display the same μ_4-κ^4-O:O′:O″:O‴ binding mode seen in **1**, **2**, and **3**, thereby forming $\{Cu_2(OCO)_4\}$ paddlewheel dimers. The internuclear distance across the dimeric units based on Cu1 is 2.6372(14) Å, with the related distance for the Cu2-based dimers being 2.6180(15) Å. The full spans of the exotetradentate adp-A and adp-B ligands form $[Cu_2(adp)_2]_n$ 1-D chain motifs very similar to that of the glutarate congener **3**, but with one extra methylene carbon in each aliphatic chain subunit.

In a similar fashion to **3**, the 3-pmna ligands in **6** exhibit a *syn* conformation (N···C_{arom}···C_{arom}···N torsion angle = 9.2°), again permitting the dipyridyl tethers to bridge copper atoms within the resulting $[Cu_2(adp)_2(3\text{-pmna})]_n$ 1-D ribbon motif (Fig. 9b) and thereby avoiding higher dimensionality. The 3-pmna ligands in **6** span a Cu···Cu distance of 8.260 Å, matching the closest interdimer

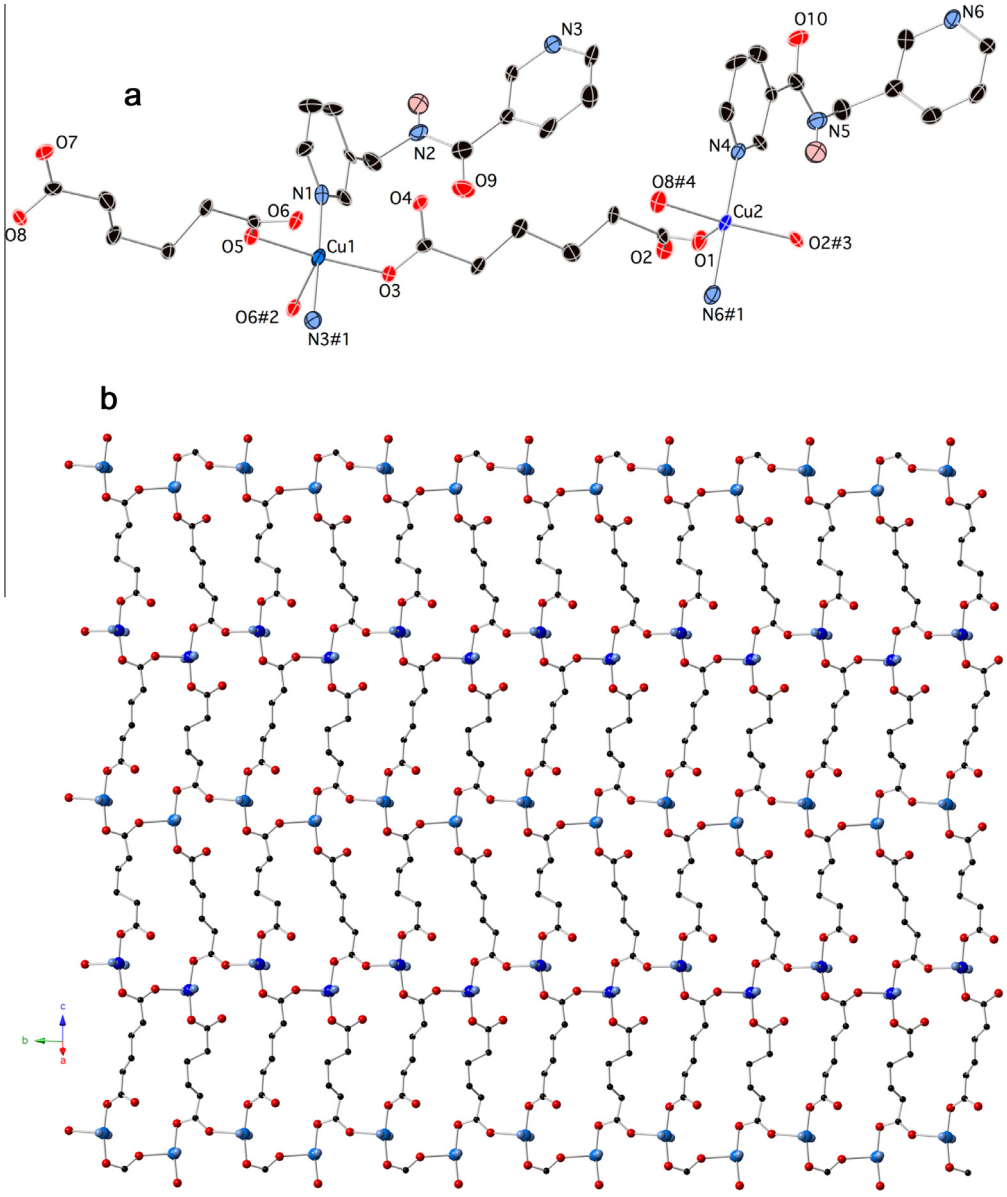

Fig. 7. (a) Coordination environment in **5** and (b) $[Cu_2(adp)_2]_n$ layer in **5**, with embedded *anti-syn* bridged $\{CuOCO\}_n$ chains.

Table 6
Selected bond distance (Å) and angle (°) data for **5**.

Cu1–O3	1.934(6)	Cu2–O1	2.283(7)
Cu1–O5	1.966(6)	Cu2–O2$^{\#3}$	1.943(6)
Cu1–O6$^{\#1}$	2.329(6)	Cu2–O8$^{\#4}$	1.943(6)
Cu1–N1	2.013(9)	Cu2–N4	2.009(8)
Cu1–N3$^{\#2}$	2.035(8)	Cu2–N6$^{\#2}$	2.039(9)
O3–Cu1–O5	168.4(3)	O2$^{\#3}$–Cu2–O1	97.5(3)
O3–Cu1–O6$^{\#1}$	91.7(3)	O2$^{\#3}$–Cu2–N4	90.4(3)
O3–Cu1–N1	93.2(3)	O2$^{\#3}$–Cu2–N6$^{\#2}$	89.3(3)
O3–Cu1–N3$^{\#2}$	88.5(3)	O8$^{\#4}$–Cu2–O1	94.9(3)
O5–Cu1–O6$^{\#1}$	99.4(3)	O8$^{\#4}$–Cu2–O2$^{\#3}$	167.6(3)
O5–Cu1–N1	89.6(3)	O8$^{\#4}$–Cu2–N4	89.5(3)
O5–Cu1–N3$^{\#2}$	88.7(3)	O8$^{\#4}$–Cu2–N6$^{\#2}$	90.7(3)
N1–Cu1–O6$^{\#1}$	92.4(3)	N4–Cu2–O1	87.2(3)
N1–Cu1–N3$^{\#2}$	178.3(3)	N4–Cu2–N6$^{\#2}$	179.3(3)
N3$^{\#2}$–Cu1–O6$^{\#1}$	87.6(3)	N6$^{\#2}$–Cu2–O1	93.5(3)

Symmetry transformations to generate equivalent atoms: #1 $-x+2, -y, -z+1$; #2 $x+1, y, z$; #3 $-x+1, -y-1, -z+2$; #4 $-x+2, -y-1, -z+1$.

Cu···Cu contact along the ribbon motifs (Fig. 5c). The longer Cu···Cu interdimer contact bridged by the adp ligands, which measures 9.609 Å, is too long to be bridged the *syn* conformation 3-pmna ligands.

Parallel sets of $[Cu_2(adp)_2(3\text{-pmna})]_n$ 1-D ribbons are connected into supramolecular layers (Fig. S6) by means of non-classical C–H···O interactions (C–O distance = 3.31(1) Å). These are in evidence between methylene carbon atoms belonging to the *gauche* part of the adp-B ligands in one ribbon, and the carboxylate oxygen atoms at the *gauche* terminus of adp-B ligands in the next ribbon. These supramolecular layers are arranged in an *ABAB* pattern, stacking along the *c* crystal direction. The ribbon motifs in neighboring supramolecular layers are oriented orthogonally to each other (Fig. S7), in contrast to the related glutarate phase **3** in which all chain submotifs are oriented parallel to each other. The partially occupied water molecules of crystallization are located in small pockets totaling 4.7% of the unit cell volume.

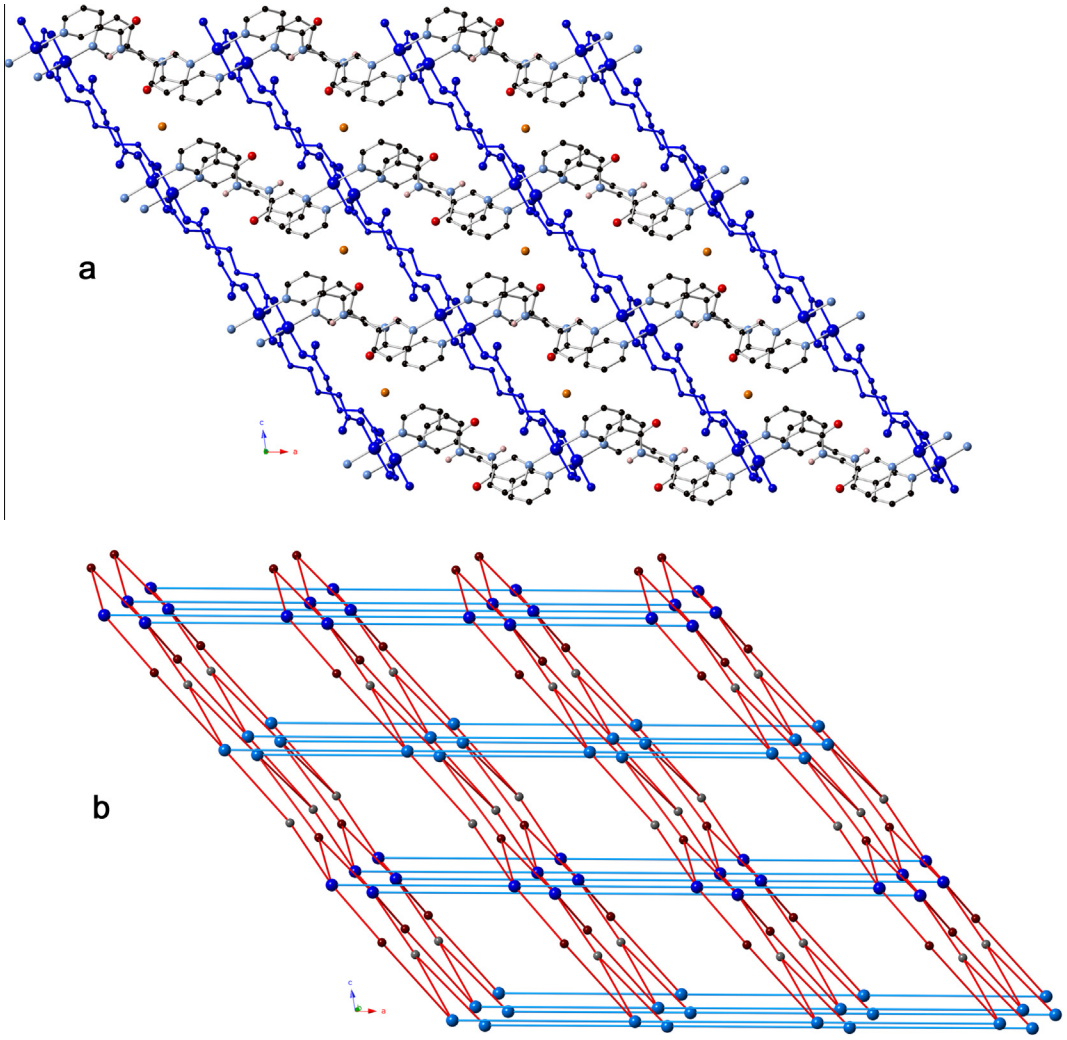

Fig. 8. (a) $\{[Cu_2(adp)_2(3\text{-pmna})_2]\cdot H_2O\}_n$ 3-D coordination polymer network in **5** and (b) Schematic perspective of the rare 3-D 3,5-connected **hms** net with $(6^3)(6^98)$ topology in **5**.

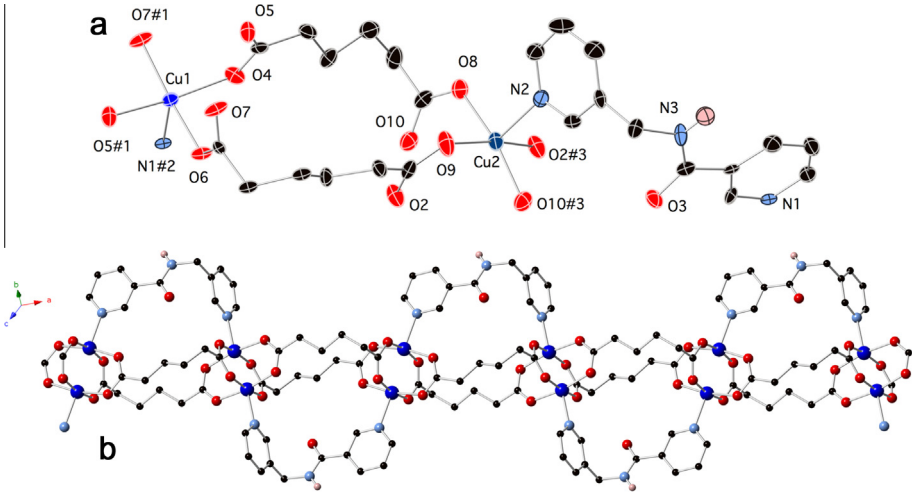

Fig. 9. (a) Coordination environments in **6** and (b) $[Cu_2(adp)_2(3\text{-pmna})]_n$ chain motif in **6** with embedded $\{Cu_2(OCO)_4\}$ paddlewheel dimers and curled conformation 3-pmna ligands.

Table 7
Selected bond distance (Å) and angle (°) data for **6**.

Cu1–O4	1.980(3)	Cu2–O8	1.961(3)
Cu1–O7$^{\#1}$	1.961(3)	Cu2–O10$^{\#2}$	1.959(4)
Cu1–O6	1.989(3)	Cu2–O9	1.979(3)
Cu1–N1$^{\#2}$	2.179(4)	Cu2–N2	2.185(4)
Cu1–O5$^{\#1}$	1.963(3)	Cu2–O2$^{\#2}$	1.981(3)
O4–Cu1–O6	88.61(13)	O8–Cu2–O9	89.23(16)
O4–Cu1–N1$^{\#2}$	94.60(13)	O8–Cu2–N2	98.67(14)
O7$^{\#1}$–Cu1–O4	90.85(14)	O8–Cu2–O2$^{\#2}$	90.05(15)
O7$^{\#1}$–Cu1–O6	168.00(13)	O10$^{\#2}$–Cu2–O8	168.73(14)
O7$^{\#1}$–Cu1–N1$^{\#2}$	100.88(13)	O10$^{\#2}$–Cu2–O9	89.48(15)
O7$^{\#1}$–Cu1–O5	87.89(14)	O10$^{\#2}$–Cu2–N2	92.52(15)
O6–Cu1–N1$^{\#2}$	91.11(13)	O10$^{\#2}$–Cu2–O2$^{\#2}$	89.01(15)
O5$^{\#1}$–Cu1–O4	168.32(13)	O9–Cu2–N2	90.13(14)
O5$^{\#1}$–Cu1–O6	90.22(13)	O9–Cu2–O2$^{\#2}$	168.64(14)
O5$^{\#1}$–Cu1–N1$^{\#2}$	97.04(13)	O2$^{\#2}$–Cu2–N2	101.18(14)

Symmetry transformations to generate equivalent atoms: #1 $-x+3/2$, $-y+3/2$, $-z+1$; #2 $-x+2$, $-y+2$, $-z+1$.

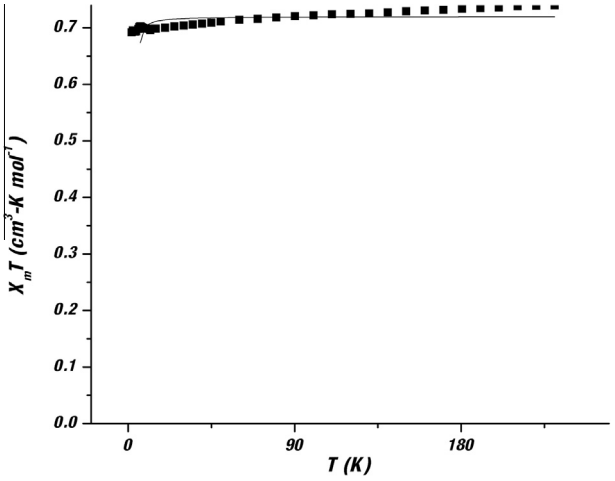

Fig. 10. Variable temperature magnetic susceptibility plot for **5**. The best fit to Eq. (1) is shown as a thin black line.

4.8. Thermogravimetric analysis

To probe the decomposition behavior of the coordination polymers prepared in this study, thermogravimetric analysis was undertaken on polycrystalline samples of compounds **1**–**5**. The mass of compound **1** remained stable until ~200 °C. Its final mass remnant at 600 °C was 23.5%, consistent with deposition of Cu metal (calc'd 22.2%). Compound **2** underwent dehydration between ~20 °C and ~95 °C, as evidenced by a mass loss of 10.3% (calc'd 12.0%). The mass remained stable until ~210 °C, whereupon ligand combustion occurred. Its final mass remnant at 600 °C was 21.6%, consistent with a mixture of CuO (calc'd 22.7%) and Cu_2O (calc'd 20.4%). Compound **3** lost its water molecules of crystallization between 180 and 220 °C, with a mass loss of 3.5% roughly consistent with the predicted value of 2.9%. The organic ligands were ejected above 220 °C. Its final mass remnant at 600 °C was 26.6%, consistent with deposition of CuO (calc'd 25.7%). The organic components of compound **4** were ejected above 220 °C. Its final mass remnant at 600 °C was 17.7%, consistent with possible deposition of a mixture of Cu_2O (calc'd 17.0%) and CuO (calc'd 19.0%). Compound **5** underwent apparent dehydration and partial decarboxylation between 20 and 115 °C, with a mass loss of 9.7%. Calculated mass values for loss of the water molecules of crystallization and two equivalents of CO_2 are 2.1% and 10.2%. Complete ejection of the organic components occurred above 210 °C. The final mass remnant at 600 °C was 12.6%, consistent with possible deposition of Cu metal (calc'd 14.8%). Unfortunately the final residues of the thermal analyses were not sufficient in quantity for PXRD characterization. Thermograms for **1**–**5** are shown in Figs. S8–S12 in the Supplementary Information.

4.9. Variable temperature magnetic study of *5*

Variable temperature magnetic susceptibility was acquired for a polycrystalline sample of **5** to probe the extent of magnetic interaction between paramagnetic divalent copper atoms along its *anti-syn* bridged $\{CuOCO\}_n$ 1-D chain submotifs. The magnetic susceptibility data followed the Curie–Weiss law (Fig. S13), with $C = 0.746$ cm^3-K/mol, consistent with the expected value for two uncoupled $S = 1/2$ ions per formula unit. The Weiss constant Θ had a value of −0.88 K, indicative of net antiferromagnetic coupling between adjacent copper ions. The $\chi_m T$ value of 0.752 cm^3-K/mol at 230 K was consistent with the expected value for $g = 2$. This value decreased slightly to 0.703 cm^3-K/mol at 25 K and 0.693 cm^3-K/mol at 2 K. The magnetic susceptibility data were also fit to Bonner and Fisher's series expansion [29] for an isotropic Heisenberg 1-D $S = 1/2$ chain (Eq. (1)). The best fit to the observed data (Fig. 12) gave $g = 1.96(3)$, and $J = -0.04(8)$ cm^{-1} with $R = 2.2 \times 10^{-2} = \{\sum [(\chi_m T)_{obs} - (\chi_m T)_{calc}]^2 / \sum [(\chi_m T)_{obs}]^2\}$. The fit was mediocre due to the extremely small value of J. The g value is in the usual range for a d^9 Cu^{2+} ion, and the very small and negative J value corroborates the presence of very weak antiferromagnetic superexchange occurring along *anti-syn* bridged $\{CuOCO\}_n$ 1-D chain submotifs in **5**. By analogy with previously reported $\{CuOCO\}_n$ 1-D chains [15], the *apical-basal* carboxylate bridges can promote weak ferromagnetic coupling, while overlaps between d_{x2-y2} orbitals on neighboring copper atoms pyramidal geometry promote antiferromagnetic coupling. In this case, the antiferromagnetic interactions predominate, plausibly due to the fairly significant deviations from square pyramidal geometry that permit overlap of neighboring d_{x2-y2} orbitals (Fig. 10).

$$\chi_m T = \frac{2Ng^2\beta^2}{k}\left(\frac{0.25 + 0.074975x + 0.075235x^2}{1 + 0.9931x + 0.172135x^2 + 0.757825x^3}\right) \quad (1)$$

with $x = J/kT$

5. Conclusions

Synergistic structure directing effects of conformationally flexible aliphatic dicarboxylate ligands and the seldom used hydrogen-bonding capable ditopic tether 3-pyridylmethylnicotinamide have permitted the self-assembly of a series of divalent cooper coordination polymers. When succinate-type dicarboxylates were employed in the synthetic attempts, the presence of two methyl substituents did not appreciably alter the coordination polymer topology from **1** to **2**. However the sterically more demanding 2,2-dimethylsuccinate ligand resulted in larger interlamellar regions in **2** that entrapped disordered water molecules of crystallization. Expansion of the dicarboxylate chain by one or two carbon atoms resulted in a reduction in dimensionality to a simple chain, as the span between the pyridyl nitrogen atoms of the 3-pmna ligands in *syn* conformation matched well with the length of the open conformation glutarate ligands in **3** or the curled conformation adipate ligands in the minor product **6**. Inclusion of a methyl group in a glutarate-type ligand resulted in an increase in dimensionality in **4** to a seldom-encountered binodal 2-D layer topology, counter to previously recognized trends in coordination polymer structural chemistry. The major product **5** from the reaction attempts with the adipate ligands shown a similar 2-D copper carboxylate layer as **4**, but the 3-pmna ligands serve as pillaring

ligands, thus forming a very rare 3-D **hms** net topology. In conclusion, 3-pyridylmethylnicotinamide has proven to be a very useful dipyridyl-type coligand for the construction of a series of structurally diverse coordination polymers.

Acknowledgments

We acknowledge Lyman Briggs College of Michigan State University for funding this work. We thank Mr. Rui Huang and Ms Jessica Mizzi for experimental assistance.

Appendix A. Supplementary material

CCDC 1010681, 1010682, 1010683, 1010684, 1010685, and 1013602 contain the supplementary crystallographic data for **1**–**6**. These data can be obtained free of charge from The Cambridge Crystallographic Data Centre via www.ccdc.cam.ac.uk/data_request/cif. Supplementary data associated with this article can be found, in the online version, at http://dx.doi.org/10.1016/j.ica.2014.08.059.

References

[1] L.J. Murray, M. Dinca, J.R. Long, Chem. Soc. Rev. 38 (2009) 1294. and references therein.
[2] J.R. Li, R.J. Kuppler, H.C. Zhou, Chem. Soc. Rev. 38 (2009) 1477 (and references therein).
[3] (a) M. Plabst, L.B. McCusker, T. Bein, J. Am. Chem. Soc. 131 (2009) 18112; (b) Y. Liu, V.C. Kravtsov, M. Eddaoudi, Angew. Chem., Int. Ed. 47 (2008) 8446; (c) F. Nouar, J. Eckert, J.F. Eubank, P. Forster, M. Eddaoudi, J. Am. Chem. Soc. 131 (2009) 18112.
[4] (a) J. Lee, O.K. Farha, J. Roberts, K.A. Scheidt, S.T. Nguyen, J.T. Hupp, Chem. Soc. Rev. 38 (2009) 1450 (and references therein); (b) L. Ma, C. Abney, W. Lin, Chem. Soc. Rev. 38 (2009) 1248 (and references therein).
[5] M.D. Allendorf, C.A. Bauer, R.K. Bhakta, R.T. Houk, Chem. Soc. Rev. 38 (2009) 1330 (and references therein).
[6] G.E. Kostakis, I.J. Hewitt, A. Ako, V. Mereacre, A.K. Powell, Phil. Trans. R. Soc. A 368 (2010) 1509.
[7] F.S. Delgado, C.A. Jimenez, P. Lorenzo-Luis, J. Pasan, O. Fabelo, L. Cañadillas-Delgado, F. Lloret, M. Julve, C. Ruiz-Perez, Cryst. Growth Des. 12 (2012) 599.
[8] P. Kanoo, R. Matsuda, M. Higuchi, S. Kitagawa, T.K. Maji, Chem. Mater. 21 (2009) 5860.
[9] (a) Y. Zheng, Z. Kong, Z. Anorg, Allg. Chem. 629 (2003) 1469; M.R. Montney, S. Mallika Krishnan, N.M. Patel, R.M. Supkowski, R.L. LaDuca, Cryst. Growth Des. 7 (2007) 1145; (c) D.P. Martin, R.M. Supkowski, R.L. LaDuca, Polyhedron 27 (2008) 2545.
[10] (a) B. Rather, M.J. Zaworotko, Chem. Commun. (2003) 830; (b) D.P. Martin, R.M. Supkowski, R.L. LaDuca, Cryst. Growth Des. 8 (2008) 3518.
[11] (a) R. Hu, Y. Kang, J. Zhang, Z. Li, Y. Qin, Y. Yao, Z. Anorg, Allg. Chem. 631 (2005) 3053; (b) A. Banisafar, D.P. Martin, J.S. Lucas, R.L. LaDuca, Cryst. Growth Des. 11 (2011) 846.
[12] K.A. Brown, D.P. Martin, R.M. Supkowski, R.L. LaDuca, CrystEngComm 10 (2008) 846.
[13] K. Uemura, K. Saito, S. Kitagawa, H. Kita, J. Am. Chem. Soc. 128 (2006) 16122.
[14] T.S. Gardner, E. Wenis, J.J. Lee, J. Org. Chem. 19 (1954) 753.
[15] O. Kahn, Molecular Magnetism, VCH Publishers, New York, 1993.
[16] SAINT, Software for Data Extraction and Reduction, Version 6.02; Bruker AXS Inc., Madison, WI, 2002.
[17] SADABS, Software for Empirical Absorption Correction. Version 2.03; Bruker AXS Inc., Madison, WI, 2002.
[18] G.M. Sheldrick, SHELXTL, Program for Crystal Structure Refinement, University of Göttingen, Göttingen, Germany, 1997.
[19] O.V. Dolomanov, L.J. Bourhis, R.J. Gildea, J.A.K. Howard, H. Puschmann, J. Appl. Cryst. 42 (2009) 229.
[20] G.M. Sheldrick, CELLNOW, University of Göttingen, Göttingen, Germany, 2003.
[21] H.D. Flack, Acta Crystallogr. A29 (1983) 876.
[22] M. Kurmoo, C. Estournes, Y. Oka, H. Kumagai, K. Inoue, Inorg. Chem. 44 (2005) 217.
[23] A.W. Addison, T.N.J. Rao, J. Reedijk, J. van Rijn, G.C. Verschoor, J. Chem. Soc., Dalton Trans. (1984) 1349.
[24] A.L. Spek, PLATON, A Multipurpose Crystallographic Tool, Utrecht University, Utrecht, The Netherlands, 1998.
[25] V.A. Blatov, A.P. Shevchenko, D.M. Proserpio, Cryst. Growth Des. 14 (2014) 3576. TOPOS software is available for download at: http://www.topos.ssu.samara.ru.
[26] Q. Chu, Z. Su, J. Fan, T. Okamura, G. Lv, G. Liu, W. Sun, N. Ueyama, Cryst. Growth. Des. 11 (2011) 3885.
[27] (a) D.S. Zhou, F.K. Wang, S.Y. Yang, Z.X. Xie, R.B. Huang, CrystEngComm 11 (2009) 2548; (b) A.L. Pochodylo, R.L. LaDuca, CrystEngComm 13 (2011) 2249.
[28] C. Gao, S. Liu, L. Xie, Y. Ren, J. Cao, C. Sun, CrystEngComm 9 (2007) 545.
[29] J.C. Bonner, M.E. Fisher, Phys. Rev. A135 (1964) 640.